



Article

# Rolling Eccentric Steel Rings on an Industrial Radial–Axial Ring Rolling Mill

Mirko Gröper <sup>\*</sup>, Marten Quadfasel, David Bailly and Gerhard Hirt

Institute of Metal Forming, RWTH Aachen University, 52072 Aachen, Germany;  
david.bailly@ibf.rwth-aachen.de (D.B.); gerhard.hirt@ibf.rwth-aachen.de (G.H.)

\* Correspondence: mirko.groeper@ibf.rwth-aachen.de; Tel.: +49-(0)241-8090093

**Abstract:** Various industries, including mechanical engineering, utilize steel rings featuring variable cross-sectional profiles, such as eccentric rings. Presently employed methods for producing eccentric rings possess drawbacks like restricted geometries, significant material wastage or uneven microstructures. The radial–axial ring rolling process serves to create seamless rolled steel rings with near-net-shaped cross-sections. A novel technique involves achieving eccentricity by dynamically adjusting the mandrel’s position during the ring rolling process. This method’s fundamental feasibility has previously been showcased using a blend of oil clay and a labor test bench. Transferring the possibility of manufacturing eccentric rings on industrial radial–axial ring rolling mills would expand the product range of ring manufacturers without encountering drawbacks associated with existing manufacturing processes. The objective of this paper is to demonstrate the basic feasibility of the concept of an industrial radial–axial ring rolling mill. In the first step, FEA simulation studies were carried out to develop the rolling strategy and estimate the achievable eccentricity on the institute’s radial–axial ring mill. Subsequently, the rolling strategy was implemented on an industrial ring rolling mill with the help of a unique technology module programmed in C++. Finally, an eccentric ring was ring rolled and compared with the FEA simulation, and the reproducibility was demonstrated to be successful.

**Keywords:** bulk metal forming; ring rolling; eccentric ring rolling; industrial process control; FEA



**Citation:** Gröper, M.; Quadfasel, M.; Bailly, D.; Hirt, G. Rolling Eccentric Steel Rings on an Industrial Radial–Axial Ring Rolling Mill. *J. Manuf. Mater. Process.* **2024**, *8*, 75. <https://doi.org/10.3390/jmmp8020075>

Academic Editors: Arkadiusz Gola, Izabela Nielsen and Patrik Grznár

Received: 5 March 2024

Revised: 3 April 2024

Accepted: 11 April 2024

Published: 12 April 2024



**Copyright:** © 2024 by the authors. Licensee MDPI, Basel, Switzerland. This article is an open access article distributed under the terms and conditions of the Creative Commons Attribution (CC BY) license (<https://creativecommons.org/licenses/by/4.0/>).

## 1. Introduction

Ring rolling is a proven bulk metal-forming process for producing large seamless rings used in safety-critical components such as in the energy, automotive and aerospace sectors [1]. Typical applications are bearings, connection flanges in wind turbines [2] or components of aircraft turbines [3]. Aside from the excellent durability of ring-rolled products, the technique is also known for its exceptional material efficiency, particularly when creating non-rectangular, near-net-shaped cross-sectional products [4].

Due to the constant cost pressure on industrial companies, new approaches for saving energy and material by extending the geometric spectrum of ring rolling have been researched in recent years (cf., e.g., [5,6]). Here, the idea of rolling non-axially symmetrical rings opens up a new possibility for saving material and energy costs. Eccentric rings could be used, e.g., in triple-ring eccentric bearings (cf. Figure 1). The material savings to be achieved and, thus, the energy savings depend on the difference between the thickest and thinnest wall thickness.

Today, eccentric rings can be machined from a solid ring, open die forged or cast. However, each of these processes offers its disadvantages, such as high machining costs, the associated high generation of scrap and long process times, as well as inflexibility due to the die or a comparatively poorer microstructure than in ring rolling [1]. Therefore, a high potential for material and energy savings arises while meeting the customer’s product-specific mechanical requirements. Due to its high flexibility, the ring rolling process offers

the possibility of producing non-axially symmetrical rings without set-up times, i.e., for changing tools and with material and energy cost savings. For this purpose, the mandrel roll of a conventional industrial radial-axial ring rolling mill must be moved dynamically based on the ring's current position and rotation angle to narrow or, respectively, enlarge the radial roll gap (cf. Figure 2, red arrow). The dynamic feed of the mandrel thus creates a ring with a circumferentially variable wall thickness.

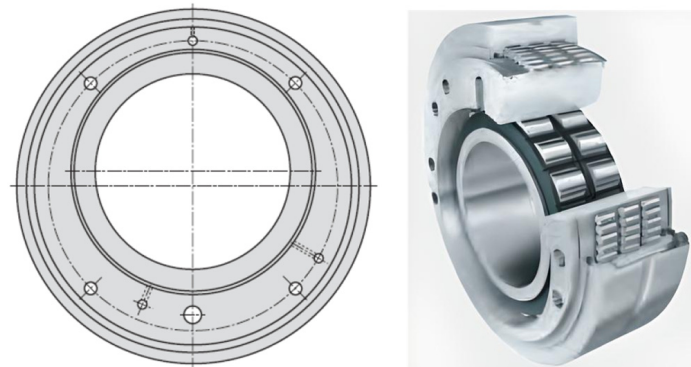


**Figure 1.** Application example: FAG three-ring eccentric bearing [7] and bearing with eccentric center and outer ring [8] used in printing machines.

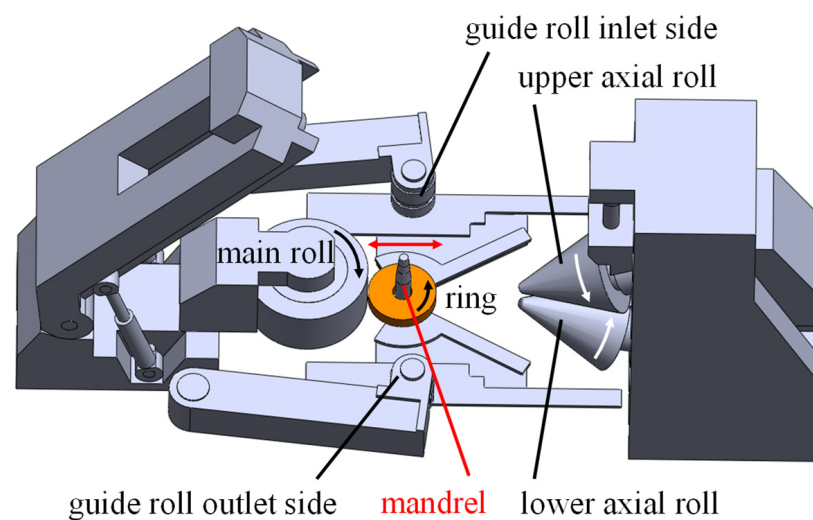


**Figure 2.** Schematic representation of a radial-axial ring rolling mill with the dynamic change of direction of the mandrel marked in red.

A method for producing rings with circumferential variable wall thickness was already discussed by Cleaver et al. [9] using a model ring rolling mill and model materials like plasticine at room temperature [10]. There were two differences between the used test bench and an industrial ring rolling mill. First, the guide rolls were not used, and the ring was centered due to differential velocity control of the axial roll. The current state of the ring geometry was measured by tracking marks on the top of the ring using a USB webcam [11]. Furthermore, the mandrel and main roll were moved together along the X-axis to keep the ring in the center of the rolling mill [9]. However, in industrial radial-axial ring rolling mills, there is a notable obstruction in viewing the ring caused by the tight closure of the tools. Additionally, substantial volumes of water steam and dust present significant challenges for optical measurements and hinder the performance of image recognition algorithms.

The current state of wall thickness in the radial roll gap must be known at all times during ring rolling to dynamically feed the mandrel at the right moment, either in the

direction of the main roll or backward. In past work [12], there was a measurement procedure rolled out using the measurement of both guide roll velocities (cf. Figure 3) to determine the position of the ring and, thus, respectively, the wall thickness in the radial rolling gap. It opened up the possibility of adjusting the mandrel's position in the right direction to form an eccentric ring on an industrial radial–axial ring rolling mill with hot steel.

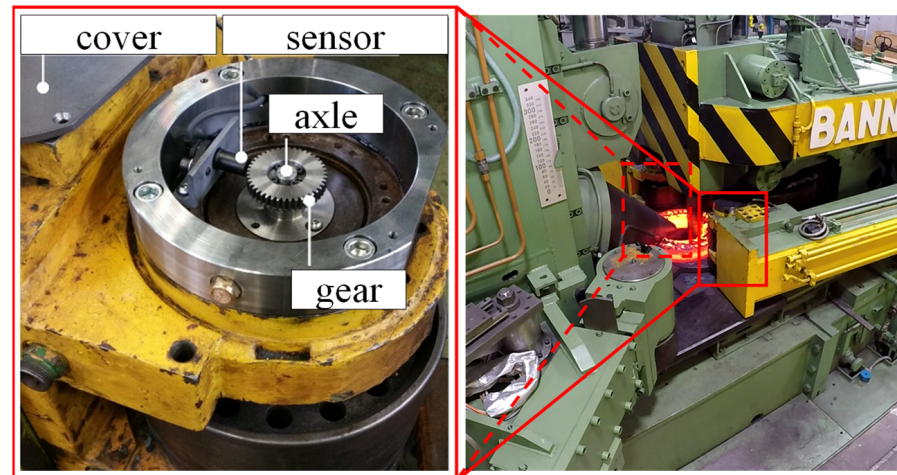


**Figure 3.** Measurement system for tracking the circumferential velocities of both guide rolls to determine the respective wall thickness in the radial gap.

Currently, there is no established rolling concept for industrial implementation. Furthermore, the factors influencing the achievable minimum and maximum achievable wall thickness difference on an industrial rolling mill remain unidentified. These gaps in knowledge underscore the need for further research and development in the field of ring rolling. Establishing an eccentric ring rolling concept for industrial application would open up material and energy cost savings. Moreover, understanding the factors that affect the range of achievable wall thickness differences is crucial for optimizing the process and enhancing its efficiency and effectiveness in industrial settings. Addressing these gaps could facilitate the adoption of eccentric ring rolling in various industrial sectors.

Therefore, in this work, the eccentric ring rolling process on an industrial radial–axial ring rolling mill is presented. Based on the measuring method described above, the eccentric ring rolling strategy was developed. Process limits and parameters for experimental realization were determined through FEA simulations. Finally, the process strategy was validated and compared with the experimental results on the industrial test bench of the Institute of Metal Forming (IBF).

## 2. The Eccentric Ring Rolling Process

The eccentric shape is formed from a concentric ring with a radius of  $r_c$ . It eliminates the need for additional operations to produce a specialized preform. Furthermore, no particular alignment of the ring needs to be made prior to the ring rolling, as would be the case with an eccentrically perforated preform. When rolling eccentric rings, it is necessary to change the direction of movement of the mandrel during ring rolling. To achieve the desired wall thickness profile (cf. Figure 4, 1), during a first half-ring revolution, the mandrel is moved in a radial direction toward the main roll (movement from C to A). During the process, the roll gap is increasingly narrowed with increasing wall thickness reduction up to a minimum wall thickness of  $s_{min}$ . In the second half-ring revolution, the mandrel is retracted accordingly with decreasing wall thickness reduction until it reverses again at a maximum wall thickness  $s_{max}$  (movement from A to C). Consequently, the initial inner radius  $r_c$  is successively increased by eccentricity  $e = (s_{max} - s_{min})/2$  in one direction (cf. Figure 4, 2). The preform for eccentric ring rolling must be selected so that the volume of the

preform is equal to that of the eccentric ring. In the calculation, it is important to consider that the eccentric end contour has a mean wall thickness of  $\bar{s} = (s_{max} + s_{min})/2$  around the circumference, as the two halves of the ring have symmetrical profiles. Therefore, the following applies to the preform:

$$V = \frac{\pi}{4} * (D_O^2 - D_i^2) * h \text{ with } D_i = D_O - 2 * \bar{s} \tag{1}$$

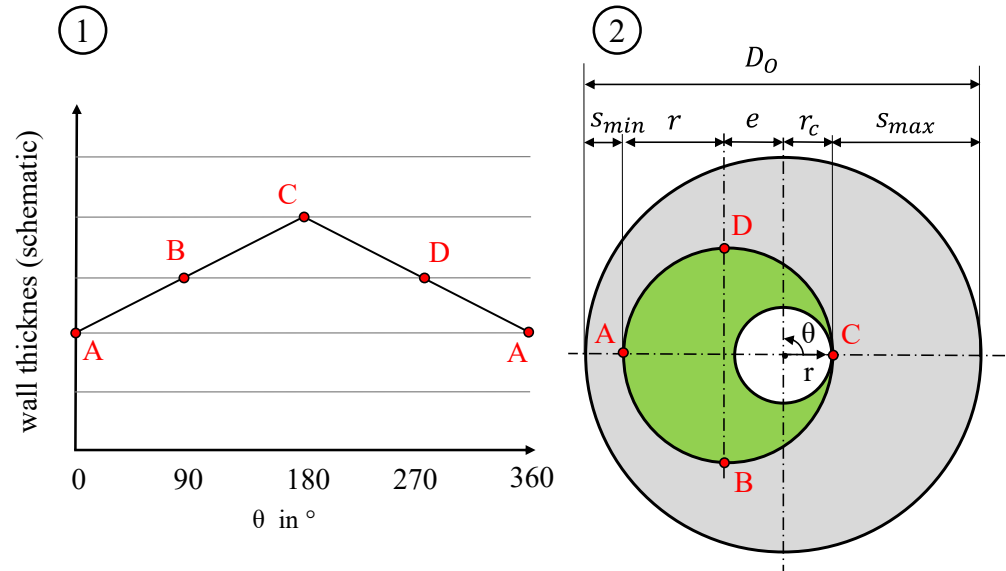


**Figure 4.** Qualitative wall thickness profile in circumferential direction (1); conceptualized eccentric ring (2).

In the first step, the hot steel ring is rolled up to an intermediate concentric shape within an expanding phase. This has the thickest wall thickness  $s_{max}$  of the eccentric rings target geometry along the entire circumference. Subsequently, the ring is rounded by a stationary mandrel for approximately two ring revolutions. After that, the eccentric ring rolling process follows (cf. flow chart in Figure 5). During the first half-ring revolution, the mandrel moves toward the main roll. During the second half-ring revolution, the mandrel's direction is reversed, moving it away from the main roll. It results in the wall thickness being progressively reduced by the mandrel's infeed during the first half-ring revolution and decreasing in the second half-ring revolution. Consequently, an approximately mirrored wall thickness profile is achieved for the ring. An exact mirroring is not achieved because the infeed constantly increases the ring diameter  $D_O$  and, thus, the half-ring rotation time  $t_{1/2}$ , as well as the translatory velocity of the mandrel. Thus, the mandrel moves between  $s_{min}$  and  $s_{max}$  within one complete ring revolution, while the height  $h$  is kept constant using the axial rolls. To achieve an increased eccentricity, the minimum wall thickness is reduced with each ring revolution until the desired target minimum wall thickness  $s_{target}$  is reached. Assuming the rotation velocity of the ring remains nearly constant, the velocity of the mandrel needs to be increased accordingly to cover the increasing distance. Once the desired minimum wall thickness  $s_{target}$  and outside diameter  $D_{O,target}$  are reached, the process is completed.

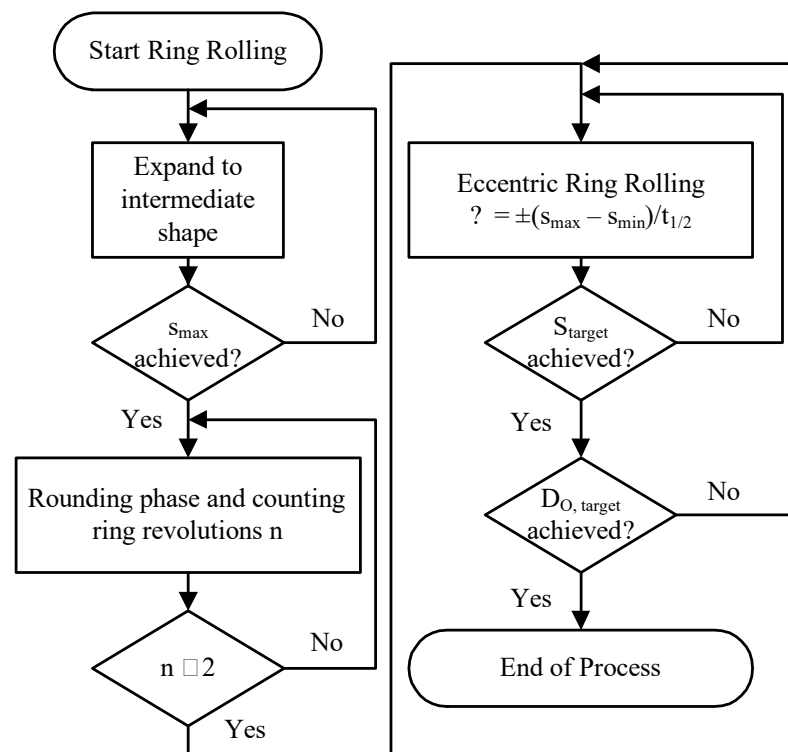


Figure 5. Flow chart of the eccentric ring rolling process.

### 3. Procedure and Influences on Eccentric Ring Rolling

FEA studies were conducted to investigate the influences on the achievable eccentricity of the eccentric ring rolling process. The start and intermediate geometries used are shown in Table 1. The material of the steel rings is construction steel (ST 37-2/1.0038 [13]). These ring geometries were selected to potentially reach the limit of mandrel kinematics. The preform was pierced in the center point. The flanks were machined and had no bulges.

Table 1. Initial and intermediate ring geometries.

Type	D <sub>O</sub>	D <sub>i</sub>	s	h
Start	420 mm	120 mm	150 mm	80 mm
Intermediate	506 mm	120 mm	99.6 mm	80 mm

D<sub>O</sub>, outer diameter; D<sub>i</sub>, inner diameter; s, wall thickness; h, ring height.

#### 3.1. FEA Model for Developing the Ring Rolling Strategy

The thermo-mechanical FEA model based on the earlier works of Jenkouk et al. [14] built in the commercial Software ABAQUS/Explicit 2019 (cf. Figure 6) was used for the studies. The FEA model features fully closed-loop controlled tool motions and utilizes the same tool geometries as the industrial-like test bench. The closed-loop control is realized using the Abaqus Subroutine VUAMP, which was extended with mandrel kinematics to develop the ring rolling strategy for eccentric rings. The tools are modeled as analytical rigid shells with constant temperatures of  $\vartheta = 200$  °C. It is adopted because the tools are preheated in an industrial environment to prevent the workpiece from cooling down excessively. Furthermore, Table 2 provides an overview of the chosen boundary values and simulation parameters. Table 3 presents a selection of the tools’ dimensions used in the model, which are aligned with those of the IBF test bench—an industrial radial-axial ring rolling mill. Additionally, Table 4 provides an overview of the tool control in the FEA model.

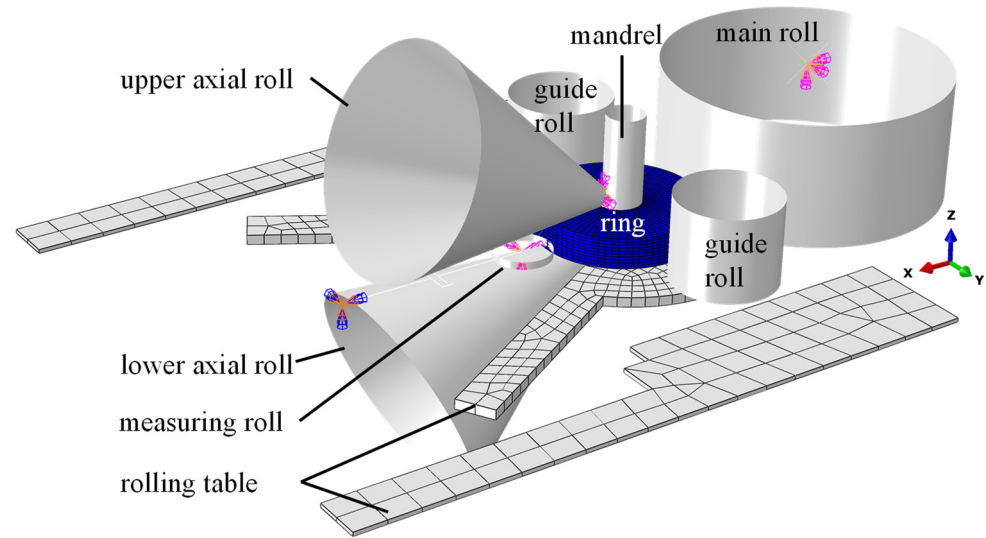


Figure 6. Set-up of the FEA model.

Table 2. Boundary values and simulation parameters.

Element Type	C3D8RT (ALE-Adaptive Mesh)
number of elements	≈15.000
emissivity	$\epsilon = 0.8$
initial ring temperatures	$\vartheta_{\text{Ring}} = 1100, 1150, 1200 \text{ }^\circ\text{C}$
mass scaling (by factor)	250
tool temperature	$\vartheta_{\text{tool}} = 200 \text{ }^\circ\text{C}$
material (yield stress)	ST 37-2 $\sigma_s = f(\varphi, \vartheta, \dot{\varphi})$
Young's modulus	$E = (\vartheta) \approx 213 \text{ kN/mm}^2$ at $1200 \text{ }^\circ\text{C}$
Poisson's ratio	$\nu = f(\vartheta) \approx 0.34$
density	$\rho = f(\vartheta) \approx 7430 \text{ kg/m}^3$ at $1200 \text{ }^\circ\text{C}$
heat capacity	$c_p = f(\vartheta) \approx 314 \text{ J/(kg K)}$ at $1200 \text{ }^\circ\text{C}$
thermal conductivity	$\lambda = f(\vartheta) \approx 39 \text{ W/(m K)}$ at $1200 \text{ }^\circ\text{C}$

Table 3. Selection of the tools' dimensions of the Banning H100/V80 mill.

Tool	Dimension
main roll:	
diameter	$D_{\text{mr}} = 748 \text{ mm}$
height	$h_{\text{mr}} = 330 \text{ mm}$
mandrel diameter	$D_{\text{md}} = 100 \text{ mm}$
guide rolls diameter	$D_{\text{gr}} = 270 \text{ mm}$
axial rolls:	
half opening angle	$\beta = 22.5^\circ$
slant height of the truncated cone	$m_{\text{ar}} = 670 \text{ mm}$
missing peak	$p_{\text{ar}} = 75 \text{ mm}$

Flow curves for the ring were generated by isothermal, frictionless, single-step compression tests for temperatures of 950–1200 °C in 50 °C steps and constant strain rates of 0.1 s<sup>-1</sup>, 1 s<sup>-1</sup> and 10 s<sup>-1</sup> at each temperature. For example, Figure 7 shows the flow curves at 1150 °C for all the strain rates. The mean values of two tests were utilized for each parameter combination of the flow curves for simulations. In the FEA model, the flow curves are represented in tabular form and automatically linearly interpolated as needed. If strains exceed the highest tabular value, the flow stress is assumed to remain constant.

**Table 4.** Kinematics of the Banning H100/V80 mill.

Tools' Motions	Description
Main roll circumferential velocity	Is kept nearly constant during ring rolling Varied between 300 and 700 mm/s
Radial mandrel velocity	Is kept nearly constant until the rounding phase Dynamic feeding in the eccentric rolling phase
Motion of both guide rolls	Is symmetrically controlled in a closed loop depending on the outer ring diameter and stabilization force (see [12,15]) Is controlled in a closed loop
Rotational speed of both axial rolls	Both rolls operate with the same rotational velocity Rotational velocity is based on the main rolls' circumferential velocity and the other diameter of the ring (see [14])
Motion of the axial rolls in radial direction	Motion depends on the outer diameter of the ring
Vertical motion of the upper axial roll	No movement; ring height is kept constant

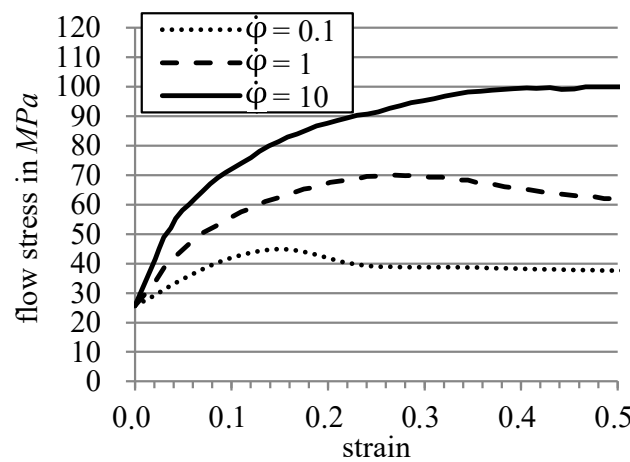


**Figure 7.** Flow curves of the construction steel (ST 37-2/1.0038) used for the FEA simulations at the forming temperature of 1150 °C for strains of 0 to 0.5. The strain rates are shown to be 0.1 s<sup>-1</sup> (dotted line), 1 s<sup>-1</sup> (dashed line) and 10 s<sup>-1</sup> (solid line).

### 3.2. Influence Parameters to Be Considered

To achieve the desired eccentricity, it is crucial to consider the performance of the rolling mill, particularly the maximum power of the hydraulic pumps  $P_{max}$ . These pumps define the kinematics of the mandrel movement. Consequently, the positioning of the mandrel is affected by the plant inertia, as the hydraulic pumps require time to accelerate or decelerate the mandrel to the required velocity or change of direction. This plant inertia can be described as the power change over time  $\Delta P = 4.85$  kW/s up to the plant's maximum and was determined empirically for the IBF ring rolling mill. Thus, the rolling mill reaches the power limit of  $P_{max} = 10$  kW in  $t_{P,max} = 2.06$  s or requires 4.12 s to accelerate and decelerate the mandrel back to a standstill. Hence, the plant inertia represents a key limiting factor for the process design in eccentric ring rolling. This is because the limit to the mandrel's translatory velocity results in the maximum achievable eccentricity. In the rolling process, the ring rotation time  $t_{rot}$  indicates the time required for a ring with the current outer radius  $r_O$  to rotate once around its axis in the ring rolling mill. The time depends on the circumferential velocity of the ring  $v_R$ , which is contributed to by the circumferential velocity of the main roll  $v_{MR}$ . Because the mandrel has to accelerate and decelerate once per half-ring revolution, the time for a half-ring revolution  $t_{1/2}$  should be greater than the time required to reach the upper power limit  $t_{P,max} = 2.06$  s in order to achieve the highest possible eccentricity. The half-ring rotation time can be estimated as follows:

$$t_{1/2} = \frac{\pi * r_O}{v_{MR}} \tag{2}$$

The ring rotation time can be increased or decreased by varying the main roll circumferential velocity. However, a reduction of the main roll circumferential velocity leads to an increase in the overall process time. In this case, the cooling of the ring during ring rolling represents a natural process limit. To investigate the impact of main roll circumferential velocity on the maximum achievable eccentricity in relation to process time, a Design of Experiment (DoE) was conducted using FEA simulations. During the investigations, the process was terminated before the thickest wall thickness was rolled over. Figure 8 shows the wall thickness applied over time at main roll circumferential velocities of 300, 400, 500 and 700 mm/s, with a reduction in the minimum wall thickness of 2.5 mm per ring revolution. The first section of the curves shows the expansion up to the intermediate geometry (Table 1) and subsequent to the eccentric rolling phase. During eccentric ring rolling, the mandrel oscillates with a constantly increasing dynamic translatory feeding rate (amplitude-like wall thickness profile). Figure 8 shows that a reduction of the circumferential velocity of the main roll increases the process time. At a main roll circumferential velocity of 300 mm/s, the highest eccentricity is achieved, indicated by the amplitude (difference between the peak and lowest point of an amplitude). The minimum and maximum wall thicknesses achieved are shown in Table 5. For the other parameters, a too-short ring rotation time led to the mandrel’s kinematic limit being reached during power build-up or, due to the plant inertia, to over-rolling of  $s_{max}$ . In this case, the control of the process terminated the respective process before the eccentricity was over-rolled. Therefore, the main roll circumferential velocity of 300 mm/s was chosen for further investigations for the specified ring geometry.

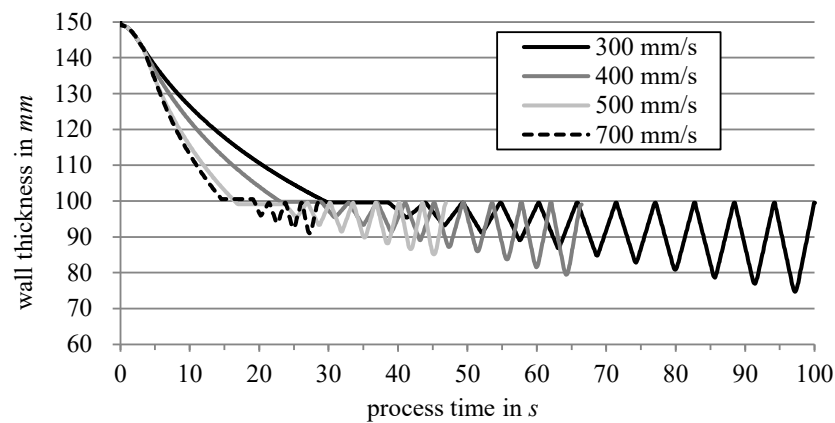


**Figure 8.** Wall thickness curves over time at main roll circumferential velocities of 300, 400, 500 and 700 mm/s.

**Table 5.**  $s_{min}$  and  $s_{max}$  at different main roll circumferential velocities and the resulting process time.

Main Roll Circumferential Velocity	$s_{min}$	$s_{max}$	Process Time
300 mm/s	74.6 mm	98.4 mm	100 s
400 mm/s	79.4 mm	98.9 mm	54 s
500 mm/s	85.1 mm	98.1 mm	47 s
700 mm/s	91.0 mm	99.4 mm	28 s

The different circumferential velocities of the main roll also influence the ring growth rate and, respectively, the change of the outer diameter over time (cf. Figure 9). This occurs because the circumferential velocity of the main roll increases the individual pass reductions on the ring, thereby increasing the single-ring growth rate. However, this can lead to a standstill of the ring in the ring rolling mill if the pass-through condition during rolling is undercut. Therefore, when reducing the main rolling velocity, it could also be necessary to reduce the ring growth rate in the expanding phase.

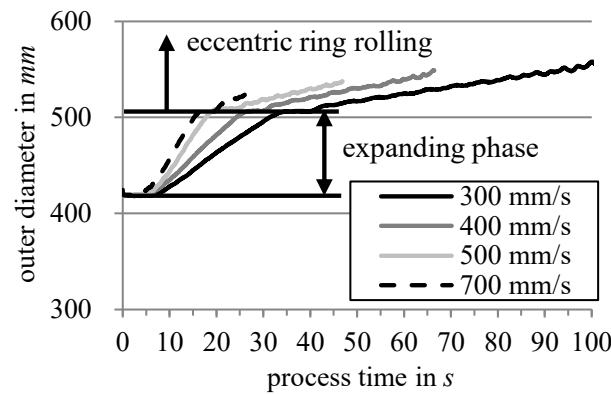


**Figure 9.** Outer diameter curves over time at main roll circumferential velocities of 300, 400, 500 and 700 mm/s.

As already mentioned, forming conditions, such as the ring temperature, have an influence on the achievable eccentricity during eccentric ring rolling, as these affect the forming force in the roll gaps. The forming force in the radial direction (short: radial force  $F_r$ ) limits the translatory feeding of the mandrel and consequently restricts the maximum achievable eccentricity.  $F_r$  depends on the geometry of the main roll and mandrel. These relations have already been described in past works such as [16,17]. The radial force can be determined approximately as a function of the mean projection of the contact area on the rolling plane  $A_r$  and the resistance of forming  $k_{w,r}$ , i.e.,  $F_r = A_r * k_{w,r}$ . Furthermore,  $k_{w,r}$  depends on the specific process and can be determined using the flow stress  $k_f$  [18]. However,  $k_f$  of the rolled material can be influenced by varying the ring temperature. Increasing process temperatures lead to a decrease in  $k_f$ , resulting in higher forming of the rolled ring when the plant limits are reached. Accordingly, Figure 10 shows the forming force for an eccentric ring rolling process in the radial gap at rolling temperatures of 1100 °C, 1150 °C and 1200 °C, with a main roll circumferential velocity of 300 mm/s from FEA simulations. The temperature curves at 1100 °C, 1150 °C and 1200 °C are shown in Figure 10. For orientation, the wall thickness curve at 1100 °C is also provided. As expected,  $F_r$  decreases with higher ring temperatures. Thus, when the force limits of the ring mill are reached, the ring temperature can be increased to reduce the required forming forces. For this reason, the maximum furnace temperature of 1226 °C was set for experimental tests. Considering the transition time of the hot ring from the oven to the ring rolling mill, the ring should have a temperature of 1200 °C.

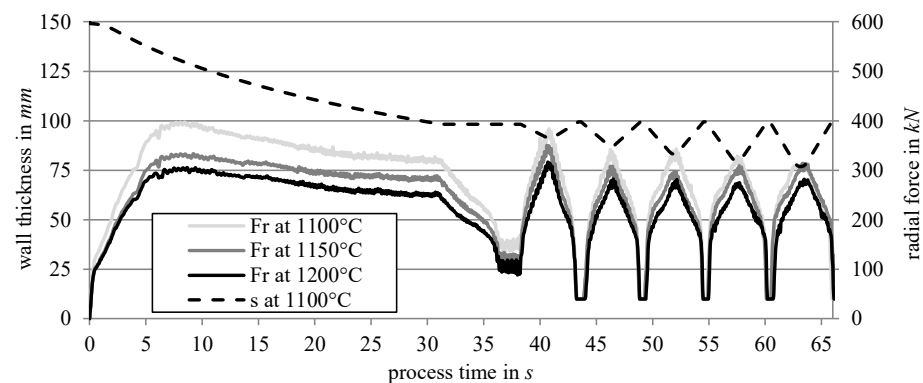


**Figure 10.** Radial force at  $\vartheta = 1100$  °C, 1150 °C and 1200 °C and  $s$  at  $\vartheta = 1100$  °C.

### 3.3. Process Parameters for Experimental Testing of the Eccentric Ring Rolling Strategy

Consequently, the main roll circumferential velocity was controlled at 300 mm/s, and the furnace temperature was set to 1226 °C. The ring geometries specified in Table 1 were used. The ring growth rate, representing the increase of the outer diameter over time,

during the expanding phase was set to 3 mm/s. The target geometry of the ring was set to  $s_{min} \leq 75$  mm, with a mandrel positioning accuracy of  $\pm 1$  mm. Additionally, the outer diameter  $D_O$  was required to be greater than or equal to 550 mm, and  $h$  was set to 80 mm.

#### 4. Experimental Validation and Results

##### 4.1. Experimental Set-Up

In order to validate the developed rolling strategy, the institute’s industrial-size ring rolling mill, Wagner Banning H100/V80, was used. The manufacturer was Wagner & Co., which now belongs to SMS Eumuco. The company is based in Witten, Germany. The maximum forces of the mill are 1000 kN in the radial direction and 800 kN in the axial direction. The test bench offers the possibility to customize the positions, velocities and rotations per minute of the tools with a unique technology module programmed in C++ (version number C++98) when there is any degree of freedom. The technology module opens up the development of an individual ring rolling strategy. The development environment used for programming is Microsoft Visual Studio 2010 Ultimate (version number 10.0.40219.1 SP1Rel).

##### 4.2. Validation Experiments of the Eccentric Ring Rolling Strategy

The eccentric ring rolling strategy, determined and optimized with FEA simulations, was implemented on the rolling mill using the technology module. The process parameters, determined with FEA simulations, were also implemented on the IBF ring mill to achieve the highest possible eccentricity. Figure 11 shows the evolution of the ring geometry over the process for different states, where  $\epsilon_V$  represents the equivalent strain. Additionally, the results of experiments conducted at the IBF ring rolling mill are presented. Table 6 provides the final geometries obtained from FEA simulation and experiments. To demonstrate the reproducibility of the process, the experiment was repeated five times. The deviation in  $e$  is a result of the summation of the deviations and scaling loss.

**Table 6.** Final eccentric ring geometries from FEA and experiments.

Type	$D_O$	$D_i$	$s_{min}$	$s_{max}$	h	e
FEA	552 mm	380 mm	74.6 mm	98.4 mm	80.0 mm	11.9 mm
Experiment no. 1	554.5 mm	381 mm	74.9 mm	97.9 mm	80.0 mm	11.5 mm
Deviation FEA/Experiment no. 1	0.45%	0.26%	0.4%	0.51%	-	3.47%
Experiment no. 2	554.5 mm	380 mm	75.0 mm	97.8 mm	80.0 mm	11.5 mm
Deviation FEA/Experiment no. 2	0.45%	-	0.53%	0.61%	-	3.47%
Experiment no. 3	554.5 mm	381 mm	75.2 mm	97.9 mm	80.0 mm	11.4 mm
Deviation FEA/Experiment no. 3	0.45%	0.26%	0.79%	0.51%	-	4.39%
Experiment no. 4	555.4 mm	379.5 mm	75.4 mm	97.7 mm	80.0 mm	11.2 mm
Deviation FEA/Experiment no. 4	0.61%	0.13%	1.06%	0.72%	-	6.25%
Experiment no. 5	554.3 mm	376.5 mm	75.2 mm	97.9 mm	80.0 mm	11.4 mm
Deviation FEA/Experiment no. 5	0.41%	0.93%	0.79%	0.51%	-	4.39%

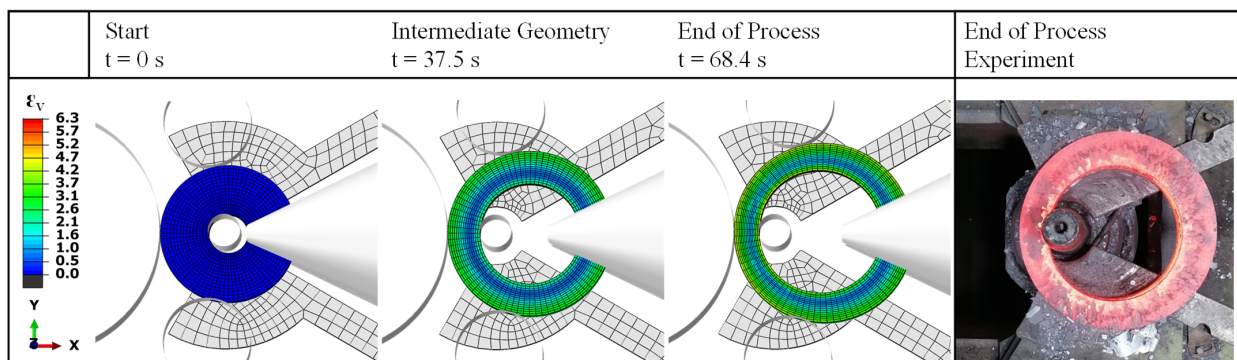


**Figure 11.** Process evolution in FEA for different time steps and rolled ring in experiment on the right.

## 5. Conclusions and Future Research Opportunities

Within this work, a new ring rolling strategy for producing eccentric rings on an industrial ring rolling mill was presented. For this, a measurement system built into the guide rolls was used to track the ring position on an industrial radial–axial ring rolling mill. FEA simulations revealed that the main roll circumferential velocity and the ring temperature significantly influence the achievable eccentricity. It was determined that the power limit and the plant inertia of the ring rolling mill are limitations when rolling eccentric rings. Furthermore, the half-ring rotation time must be longer than the time required for the plant to reach its maximum power. Additionally, increasing the ring temperature as much as possible is essential for achieving a high eccentricity. The comparison of the FEA simulation and experiments showed a maximum deviation of 6.25%. Additionally, the reproductivity of the rolling strategy was demonstrated by repeating the ring rolling process five times in experiments.

However, for an industrial implementation, an eccentric rounding phase should be added at the end of the eccentric rolling phase in order to achieve a more uniform ring geometry.

Furthermore, the ring rolling strategy should be optimized to reduce process time to obtain a higher productivity in the process. This could be achieved by decreasing the smallest wall thickness in fewer ring rotations. Furthermore, the optimization of the microstructure in the smallest area should also be focused on because of the fact that the smallest area of the ring is the weakest point on the ring. Furthermore, the rolling strategy should be transferred to larger ring geometries in order to enable a wider field of applications.

**Author Contributions:** M.G.: Conceptualization, Methodology, Coding, Formal Analysis and Investigation, Writing—Original Draft, and Writing—Review and Editing; M.Q.: Simulation, Experimental Investigation, and Writing—Review and Editing; D.B.: Writing—review and editing, Supervision; G.H.: Writing—review and editing, Supervision. All authors have read and agreed to the published version of the manuscript.

**Funding:** The work was funded by the Deutsche Forschungsgemeinschaft (DFG, German Research Foundation)—454751242.

**Data Availability Statement:** The data presented in this study are available on request from the corresponding author.

**Conflicts of Interest:** The authors declare no conflicts of interest.

## References

1. Allwood, J.; Tekkaya, E.; Stanistreet, T.F. The development of Ring rolling technology. *Steel Res. Int.* **2005**, *76*, 111–120. [CrossRef]
2. Lee, Y.S.; Lee, M.W.; Park, S.S.; Lee, I.; Moon, Y.H.; Lee, M.G. Process Design by FEM Simulation for Shape Ring Rolling of Large-Sized Ring. In Proceedings of the 10th International Conference on Numerical Methods in Industrial Forming, Pohang, Republic of Korea, 13–17 June 2010; pp. 964–971.
3. de Souza, U.; Pursell, Z.; Phillips, K.; Vaze, S. Profile Ringrolling: New techniques have been developed to lower the cost and improve the buy-to-fly ratio of rings and cases in aerospace engines through advances in preform design and processing. *Adv. Mater. Process.* **2003**, *161*, 35–37.
4. Keeton, C.R. Ring Rolling. In *ASM International Metals Handbook VOL 14—Forming and Forging*, 9th ed.; ASM International: Novolty, OH, USA, 1988; pp. 224–268.
5. Cleaver, C.J.; Lohmar, J.; Tamimi, S. Limits to making L-shape ring profiles without ring growth. *J. Mater. Process. Technol.* **2021**, *292*, 117062. [CrossRef]
6. Liang, L.; Guo, L.; Liu, Z.; Wang, P.; Zhang, H. On a precision forming criterion for groove-section profiled ring rolling process. *J. Mater. Process. Technol.* **2021**, *296*, 117207. [CrossRef]
7. FAG Industrial Bearings AG. FAG Triple Ring Eccentric Bearings in a Sheetfed Offset Press, 2003. Available online: [https://www.schaeffler.com/remotemedien/media/\\_shared\\_media/08\\_media\\_library/01\\_publications/schaeffler\\_2/publication/downloads\\_18/wl\\_23502\\_de\\_de.pdf](https://www.schaeffler.com/remotemedien/media/_shared_media/08_media_library/01_publications/schaeffler_2/publication/downloads_18/wl_23502_de_de.pdf) (accessed on 27 September 2023).
8. Schaeffler Technologies GmbH & Co. KG. Genauigkeitslager Für Druckmaschinen, 2023. Available online: [https://www.schaeffler.com/remotemedien/media/\\_shared\\_media/08\\_media\\_library/01\\_publications/schaeffler\\_2/tpi/downloads\\_8/tpi\\_222\\_de\\_de.pdf](https://www.schaeffler.com/remotemedien/media/_shared_media/08_media_library/01_publications/schaeffler_2/tpi/downloads_8/tpi_222_de_de.pdf) (accessed on 27 September 2023).

9. Cleaver, C.J.; Arthington, M.R.; Mortazavi, S.; Allwood, J.M. Ring rolling with variable wall thickness. *CIRP Ann. Manuf. Technol.* **2016**, *65*, 281–284. [[CrossRef](#)]
10. Arthington, M.R.; Havinga, J.; Duncan, S.R. Control of ring rolling with variable thickness and curvature. *Int. J. Mater. Form.* **2020**, *13*, 161–175. [[CrossRef](#)]
11. Arthington, M.R.; Cleaver, C.; Allwood, J.; Duncan, S. Measurement and control of variable geometry during ring rolling. In Proceedings of the 2015 IEEE Conference on Control Applications (CCA), Sydney, Australia, 21–23 September 2015; IEEE: Piscataway, NJ, USA, 2015; pp. 1448–1454.
12. Gröper, M.; Bailly, D.; Stergianou, S.; Hirt, G. Development of a measurement method for tracking the position of hot steel rings on an industrial radial-axial ring rolling mill. *WGP Prod. Eng.* **2023**, 1–11. [[CrossRef](#)]
13. Spittel, M.; Spittel, T. Steel symbol/number: S235JRG2/1.0038. In *Metal Forming Data of Ferrous Alloys—Deformation Behaviour, 2C1*; Martienssen, W., Warlimont, H., Eds.; Landolt-Börnstein-Group VIII Advanced Materials and Technologies; Springer: Berlin/Heidelberg, Germany, 2009; pp. 126–131.
14. Jenkouv, V.; Hirt, G.; Franzke, M.; Zhang, T. Finite element analysis of the ring rolling process with integrated closed-loop control. *CIRP Ann. Manuf. Technol.* **2012**, *61*, 267–270. [[CrossRef](#)]
15. Jenkouv, V.; Hirt, G.; Franzke, M. 3D-FE simulation of ring rolling with integrated closed-loop tool motion control. In Proceedings of the ICRF 2012, 1st International Conference on Ingot Casting, Rolling and Forging, Aachen, Stahleisen, Düsseldorf, Germany, 18–21 April 2012.
16. Kopp, R.; Koppers, U.; Wiegels, H. New Control System for Ringrolling. *Adv. Technol. Plast.* **1987**, *2*, 803–807.
17. Hawkyard, J.B.; Johnson, W.; Kirkland, J.; Appleton, E. Analyses for roll force and torque in ring rolling, with some supporting experiments. *Int. J. Mech. Sci.* **1973**, *15*, 873–893. [[CrossRef](#)]
18. Kopp, R. (Ed.) Umformtechnik Stahl und NE-Werkstoffe Visionen und innovative Lösungen. In Proceedings of the 19. ASK, Aachener Stahlkolloquium, Aachen, Germany, 25–26 March 2004; Eurogress Aachen Tagungsband, Verlag Mainz: Aachen, Germany, 2004.

**Disclaimer/Publisher’s Note:** The statements, opinions and data contained in all publications are solely those of the individual author(s) and contributor(s) and not of MDPI and/or the editor(s). MDPI and/or the editor(s) disclaim responsibility for any injury to people or property resulting from any ideas, methods, instructions or products referred to in the content.